Percolation and structural properties of particle deposits

H. S. Choi and J. Talbot
School of Chemical Engineering, Purdue University, West Lafayette, Indiana 47907

G. Tarjus and P. Viot
Laboratoire de Physique Théorique des Liquides, Université Pierre et Marie Curie, 4, place Jussieu 75252 Paris Cedex 05, France
(Received 29 August 1994)

We investigate the percolation properties of configurations of spherical particles deposited by a generalized ballistic deposition model. In this model, a tuning parameter a is introduced for controlling the relative efficiency of two mechanisms: direct deposition and deposition by following the path of steepest descent on previously deposited particles. Any particle that is trapped in an elevated position after rolling is rejected. Exact critical exponents are obtained for the $(1+1)$-dimensional version of the model. We performed computer simulations of the $(2+1)$-dimensional version and by studying the percolative behavior both for fixed values of a, as a function of the surface coverage θ, and along the saturation curve $\theta(a,\infty)$, we construct the percolation phase diagram of the model. Below a threshold value, $a_c \simeq 3.05$, there is no percolation transition, but we give some evidence for a "virtual percolation line." The critical exponents β,γ,ν are determined by finite-size scaling and Monte Carlo renormalization group techniques, and are shown to be consistent with those of ordinary two-dimensional lattice percolation. Finally, changes of structure with a are illustrated through the pair distribution function and the pair connectedness function.

PACS number(s): 81.15.Lm

I. INTRODUCTION

Complex structures involving clustering may be formed by the adsorption of colloidal particles as well as the growth of bacterial colonies [1–3]. These processes have many applications including chromatographic separation of proteins, formation of thin organic films, protein production from micro-organisms, and characterization of microbial colony growth. Despite this, modeling and theoretical studies of the kinetics and the structure of these processes have received less attention than the experimental studies. Many experimental observations [4–7] suggest that two factors are of great importance, namely the geometric exclusion effects and the irreversible nature of the deposition processes. Accordingly, the adsorption of colloidal particles has been often analyzed with the help of the random sequential adsorption (RSA) model [3–8], in which hard particles are deposited randomly, one after another, with the condition that particles overlapping the preadsorbed particles are rejected. However, RSA does not consider various interactions that adsorbing particles experience during the transport process from bulk to the surface. These interactions include dispersion, electrostatic, hydrodynamic forces, and gravity, in addition to short range repulsion. Despite its simplicity, RSA seems to be well suited to describe cases where the density difference between solvent and solute is small, as in protein adsorption [7]. In the opposite limit, in which the adsorbing particles are much denser than the solvent, their motion is strongly affected by gravity [9] and can be described, in solution, by straight line trajectories and, near the adsorbing surface, by the path of steepest descent on the previously deposited particles. In order to handle this case, a ballistic deposition (BD) model in which multilayer formation is not allowed has been introduced [10,11]. The saturation density of BD is larger than that of RSA and the saturation state is reached faster in the BD model (an exponential, instead of algebraic, time behavior) [10–13]. On the other hand, in the Eden model [14], which was developed to simulate the growth of cell colonies, the process begins from a single seed and empty surface sites are filled randomly with a probability proportional to the number of occupied nearest neighbors. A growth model similar to the Eden model, the off-lattice ballistic aggregation model, was also developed by Vold [15] to simulate colloidal aggregation: The growth process is started with a single stationary particle and other particles follow random ballistic trajectories in the vicinity of the stationary particle; if a moving particle contacts the stationary particle, it sticks at that position and a stationary cluster is formed.

The above three models (RSA, BD, and the Eden-type off-lattice ballistic aggregation model) can be combined in a generalized ballistic deposition (GBD) model [16,17], which is defined as follows. Randomly positioned spheres are dropped, one after one, from above the adsorbing plane. A sphere follows vertical trajectory until it reaches either the adsorbing plane or a preadsorbed sphere. In the first case, the trial sphere is retained with a probability $(1-p)$ or removed with a probability p. In the second case, the trial sphere follows the path of steepest descent on the previously adsorbed particles. If the particle is trapped in an elevated position, it is removed (no multilayer formation); otherwise, it is accepted with a probability p or is rejected with a probability $(1-p)$. The time evolution of the surface coverage θ is governed by the following rate equation,

$$d\theta/dt = \Phi^{DD}(\theta) + a\Phi^{RM}(\theta) , \quad (1)$$

where $\Phi^{DD}(\theta)$ is the available surface function for direct deposition (seeding process), $\Phi^{RM}(\theta)$ is that for the deposition through rolling motion (growing process) and a is defined as

$$a = \frac{p}{(1-p)} . \quad (2)$$

Hence, a is a tuning parameter that controls the efficiency of the restructuring of the adsorbed monolayer due to the motion of the adsorbing particles over the previously deposited particles. When $a=0$, the model is equivalent to RSA, since all particles can be only adsorbed by direct deposition. When $a=1$, the GBD model reduces to the simple BD model. For $a \to \infty$, it corresponds to an off-lattice ballistic aggregation model. Thus, the tuning parameter plays an important role in determining both the structure of clusters formed by deposited particles and the kinetics of the process. Viot, Tarjus, and Talbot [16] obtained the analytical solution of the $(1+1)$-dimensional GBD model and Tarjus *et al.* [17] studied both the initial regime and the asymptotic kinetics of the $(2+1)$-dimensional GBD model. It was observed in the latter study that low coverage expansions of the kinetics, which are very efficient to RSA [8], describe a range of coverage, which shrinks as a becomes larger. Similarly, the asymptotic regime, which represents in practice a sizable fraction of the saturation coverage for RSA, describes a rapidly decreasing part of the process as a increases. Thus, theoretical methods borrowed from liquid-state physics and geometrical analysis of the configurations on the surface are not sufficient when cooperative effects become more important and longer ranged. The emergence of such effects in the GBD model are related to the existence of a percolation transition.

Percolation theory has played an important role in a variety of physical problems like the sol-gel transition and transport phenomena (such as conduction or diffusion) within fractal structures [1,18–21]. While percolation in various lattice systems has been extensively investigated [18–22], continuum percolation has received comparatively less attention [23–26]. Nevertheless, it has been reported that the static exponents (β, γ, and ν) for continuum percolation are the same as those for lattice percolation [23,27], whereas the dynamic exponents are not universal [28,29]. The theoretical studies of continuum percolation have concentrated on equilibrium models such as the penetrable-concentric shell model (PCS model) [24], which are useful for generating equilibrium particle aggregates [26] and for explaining the sol-gel transition in dense dispersions [30]. However, in many processes, such as formation of colonies of microbes and colloid adsorption on solid surface, the PCS model cannot generate the proper structures since it does not consider the irreversible nature of the processes. While the percolation transition is controlled by the density ρ and the core parameter λ in the PCS model, it is controlled by the surface coverage θ and the tuning parameter a in the GBD model.

The present work is concerned with continuum percolation of spherical particles deposited irreversibly by the generalized ballistic deposition model. Unlike other continuum systems studied so far, the entire process is irreversible and the system is modeled by hard spheres without an attractive potential well. An objective of this study is to understand the characteristics of this model through percolation theory. Thus, we investigate the critical properties and apply various techniques, such as Monte Carlo renormalization group methods and finite-size scaling, to obtain the critical exponents and to check whether irreversibility and exclusion effects change the universality class. We also construct the percolation phase diagram of this system as a function of both surface coverage θ and tuning parameter a. Finally, we discuss different structural aspects of the configurations of deposited spheres along the saturation line.

II. SIMULATION

Configurations of deposited spheres were generated by simulations in a square cell of side L with the usual periodic boundary conditions. The relative size of a sphere of diameter σ to the simulation cell is specified by the parameter $r_a=(\pi\sigma^2)/(4L^2)$ and the coverage is defined as $\theta=(N\pi\sigma^2)/(4L^2)$ where N denotes the number of deposited particles. The simulation algorithm proceeds as follows. First, a trial position within the cell is generated using a uniform random number generator. If there is no overlap between the projection of an incoming particle on the plane and the deposited particles, a uniform random number ξ is generated on the interval [0,1]. If $\xi<(1-p)$, the incoming particle is accepted. Otherwise, it is rejected. If there is any overlap in the trial position, the trial sphere may be deflected once, twice, three, or four times before reaching the surface, or it may be trapped in a stable elevated position and be rejected [13]. If the sphere reaches the surface after rolling on preadsorbed spheres, it is fixed at the position with probability p. Details of the algorithm are given elsewhere [11–13].

To determine whether any spanning cluster of directly connected spheres exists, we used the modified "graph" technique. This technique requires less computer memory than the usual graph technique. Numbers from 1 to n in order are assigned to successively adsorbed particles. If the ith particle is deposited through rolling and is connected with particle j, the graph matrix G, whose elements all have initially been set to zero, is sequentially filled with numbers that indicate the connected particles as follows:

$$G(i,k)=j , \quad 1 \le k \le 6 , \quad (3)$$

$$G(j,k')=i , \quad i \le k' \le 6 , \quad (4)$$

where k and k' are the first available memory locations. Since a particle can be connected with at most six particles in a two-dimensional (2D) system, only six memory sites for each particle are needed. For example, if a center particle i contacts three particles, the first three $G(i,k)$ contain the index numbers of these particles, while the remaining memory sites are still set to zero. However,

since the central simulation cell is surrounded by periodic replicas, one could search a wrong connection path through the boundaries. Thus, we use "free boundary conditions" [26] in determining the graph matrix, i.e., if two particles are connected through a boundary, $G(i,k)$ is not updated and still set to zero. Therefore, $G(i,k)$ indicates all particles connected with a particle i *within* the central cell. Following this procedure, the graph matrix is eventually filled with index numbers. In the meantime, all pairs of particles that are connected through periodic boundaries are monitored, $(n_1^b,n_1^t),\ldots,(n_k^l,n_k^r),\ldots,(n_m^l,n_m^r)$, where n_i^b and n_i^t are the index number of particles at the bottom and the top of the central cell, respectively, and n_j^l and n_j^r are the index number of particles at the left hand side and the right hand side of the central cell, respectively. Each one of the particles n_i^b or n_j^l becomes a starting point for a searching process. By using $G(i,k)$ as a pointer, we can visit all particles within a cluster containing one of those starting particles. We associate an index $v(i)$ to each visited particle. If a particle is visited after starting at particle n_i^b, its index value, initially set to zero, becomes 1. After all particles within the cluster are visited and the corresponding index values are set to 1, if $v(n_i^t)\neq 1$, the cluster is not spanning through the system. Otherwise, it is a spanning cluster.

Throughout the simulation we monitored the order parameter P_∞, which is defined as the probability that any particle chosen at random belongs to the infinite cluster, the susceptibility χ, and the mean cluster size S (the two latter quantities are defined for finite clusters). In continuum percolation, the variable that naturally replaces the fraction of occupied sites p of lattice percolation is the surface coverage, θ, i.e., the fraction of the total surface that is covered by the deposited particles. Near the percolation threshold θ_c, the order parameter, the susceptibility, and the mean cluster size follow power laws

$$P_\infty(\theta)\sim(\theta-\theta_c)^\beta , \quad \text{for } \theta\geq\theta_c \tag{5}$$

and

$$\chi(\theta)\sim S(\theta)\sim|\theta-\theta_c|^{-\gamma} , \tag{6}$$

above and below the critical point. Note that the susceptibility χ and the mean cluster size differ only above the percolation threshold, $\theta>\theta_c$. Another important property characterizing the critical behavior is the correlation length ξ, which is defined as the mean distance between two sites on the same (finite) cluster and has the following power law behavior:

$$\xi(\theta)\sim|\theta-\theta_c|^{-\nu} . \tag{7}$$

However, instead of computing directly the correlation length ξ, we monitored the number of realizations of a system with size L, $R(L,\theta,a)$, which has any spanning cluster at a coverage θ for a given value of a. This quantity enables one to estimate the critical exponent ν of the correlation length through Monte Carlo renormalization group theory and finite-size scaling techniques [23,25]. Moreover, the above three exponents for percolation are related by the following expression:

$$d\nu=2\beta+\gamma , \tag{8}$$

where d is the dimension of system. Since determining these exponents requires good accuracy, we carried out six sets of calculations corresponding to six system sizes ($r_a=0.0001$, 0.0002, 0.0003, 0.0005, 0.001, 0.005), with 300–1000 independent runs for each system size.

In the GBD model, percolation depends not only on the surface coverage θ, but also on the parameter a. For $a=0$ (RSA) there is no percolation transition, nor for $a=1$ (simple BD). A percolation transition appears only if clustering is strong enough, that is if a is large enough. Otherwise, the system saturates (jamming limit) with only finite-size clusters. An interesting point in the percolation phase diagram is, thus, the critical value of a at which the system can first percolate. For this value a_c, percolation occurs exactly at saturation, $\theta_c=\theta(a_c,\infty)$, and if one follows the process at constant parameter $a=a_c$, there is no percolating phase for $\theta>\theta_c$. An alternative route to investigate the critical point at a_c is to follow the behavior of the system *along the saturation line.* The two relevant variables, θ and a, are then related in a nontrivial manner and before studying the (2+1)-dimensional version of the model, we first discuss the (1+1)-dimensional version for which the analytical solution is known [16].

III. (1+1)-DIMENSIONAL GBD MODEL

An important issue in this study is the choice of the most appropriate variable along the saturation line. To obtain some insight on this, we consider the (1+1)-dimensional model for which exact analytical expressions are available for the kinetics and cluster size distributions [16]. Even though the one-dimensional layer of deposited particles does not possess percolation properties above the percolation threshold, it does allow us to study the percolation behavior along the saturation line.

In the generalized ballistic deposition model (for $a>0$), the rolling mechanism leads to the formation of clusters composed of directly connected particles, contrary to the RSA case ($a=0$). If we define $\rho_s(a,t)$ as the density of clusters of size s, the total number density of clusters is

$$n_G(a,t)=\sum_{s=1}^{\infty}\rho_s(a,t) \tag{9}$$

and the particle is

$$\rho(a,t)=\sum_{s=1}^{\infty}s\rho_s(a,t) \tag{10}$$

and, choosing σ as the unit of length, their exact analytical form can be obtained as [16]

$$\rho(a,t)=\int_0^t dt'\frac{H(t')}{t'^2}(1+2at')e^{2a(1-t'-e^{-t'})} \tag{11}$$

and

$$n_G(a,t)=\int_0^t dt'\frac{H(t')}{t'^2}e^{2a(1-t'-e^{-t'})} , \tag{12}$$

where $H(t)=\exp[-2\gamma+2\mathrm{Ei}(-t)]$, $\gamma=0.57721\ldots$ is the Euler constant, and $\mathrm{Ei}(-t)=\int_t^\infty dx\,\exp(-x)/x$ is the

exponential integral.

The particle density at saturation $\rho(a,\infty)$ increases gradually from the RSA value $[\rho_{\mathrm{RSA}}(\infty)=0.747]$ through the simple BD $[\rho_{\mathrm{BD}}(\infty)=0.808]$ to that of ballistic aggregation model $[\rho(\infty)|_{a=\infty}=1.0]$ as the tuning parameter a is increased. On the other hand, the total number density of clusters at saturation $n_G(a,\infty)$ decreases monotonically with increasing a [16].

For large values of a and $t\to+\infty$, Eqs. (11) and (12) admit the following asymptotic expansions:

$$\rho(a,\infty)=1-\tfrac{1}{4}\sqrt{\pi/a}+O(1/a)\ , \tag{13}$$

$$n_G(a,\infty)=\tfrac{1}{2}\sqrt{\pi/a}+O(1/a)\ . \tag{14}$$

The mean number of particles per cluster,

$$M(a,t)=\frac{\rho(a,t)}{n_G(a,t)} \tag{15}$$

behaves then asymptotically as

$$M(a,\infty)\sim a^{1/2}\ ,\quad \text{when } a\to\infty\ . \tag{16}$$

The preceding equation is similar to the behavior shown in a related lattice model, the 1D monomer filling with nearest-neighbor cooperativity. In the regime of strong clustering, $\alpha=k_1/k_0\gg 1$, where k_i is the rate for filling sites with already i filled neighbors and α plays the role of the tuning parameter a, the average cluster size increases in that model like $\alpha^{1/2}$ at fixed coverage [31].

Combining Eqs. (13) and (16) leads to

$$M(a,\infty)\sim[1-\rho(a,\infty)]^{-1}\ ,\quad \text{as } \rho(a,\infty)\to 1\ . \tag{17}$$

In addition to the above quantities, one can introduce the susceptibility

$$\chi(a,t)=\sum_{s=1}^{\infty}s^2\rho_s(a,t)\ , \tag{18}$$

which is the second moment of the cluster density, and the mean cluster size $S(a,t)$, distinct from $M(a,t)$, which is traditionally defined by

$$S(a,t)=\frac{\sum_{s=1}^{\infty}s^2\rho_s(a,t)}{\sum_{s=1}^{\infty}s\rho_s(a,t)}=\frac{\chi(a,t)}{\rho(a,t)}\ . \tag{19}$$

Using the exact formula given in [16] for the density of clusters $\rho_s(a,t)$, one obtains the asymptotic expression

$$S(a,\infty)\sim\begin{cases}a^{1/2}\ , & \text{as } a\to\infty\\ [1-\rho(a,\infty)]^{-1}\ , & \text{as } \rho(a,\infty)\to 1\ .\end{cases} \tag{20}$$

Similarly, one obtains that the nth moment of the cluster density at saturation $\rho_s(a,t)$ behaves asymptotically as $a^{(n-1)/2}$ when $a\to+\infty$. An obvious consequence is that the correlation length ξ goes as $a^{1/2}$ when $a\to+\infty$, or else using Eq. (13),

$$\xi\sim[1-\rho(a,\infty)]^{-1}\ ,\quad \text{as } \rho(a,\infty)\to 1\ . \tag{21}$$

Choosing the density at saturation $\rho(a,\infty)$ as the proper variable to study the percolation behavior, we thus derive from Eqs. (17), (20), and (21) that the static exponents take their usual value for 1D percolation: $\nu=\gamma=1$. If, however, we choose a, or rather the probability p defined in Eq. (2) as the relevant variable. We obtain

$$S(p)\sim\xi(p)\sim(1-p)^{-1/2}\ ,\quad \text{as } p\to 1\ , \tag{22}$$

which would lead to $\gamma=\nu=\frac{1}{2}$, in contradiction with ordinary percolation. The probability p is by no means a continuum equivalent of the occupation probability on a lattice. The apparent paradox of Eq. (22) is simply due to the nonanalytical dependence on p (or a) of the saturation density when $p\to 1$ (or $a\to+\infty$). As will be shown below, such a problem does not appears in (2+1)-dimensions since the percolation threshold occurs at a finite value of a for which a nonanalytic dependence on p or a of the saturation coverage is not expected.

IV. (2+1)-DIMENSIONAL GBD MODEL

A. System characteristics

The coalescence of two clusters is impossible in the (1+1)-dimensional GBD model because geometric constraints allow rolling over only one particle before adsorption. The (2+1)-dimensional GBD contains three additional mechanisms which correspond to two, three, and four deflections of an adsorbing particle. These three mechanisms may result in the connections between clusters, which can lead to a percolated structure of deposited particles. The connecting process is the continuum counterpart of sequential adsorption processes of monomers on two-dimensional lattices with additional cooperativities favoring deposition of monomers near two or more occupied sites [3]. There is no simple relation, however, between the rates of filling sites with i neighbors and the parameter a because in the GBD model the effective deposition rates are also determined, in a nontrivial way, by the geometry of the local configurations of adsorbed spheres.

The qualitative characteristics of the 2D GBD system are illustrated in several snapshots (Fig. 1) of saturation configurations generated with different values of a. In Fig. 1(a) ($a=1$), the cluster composed of black spheres is the largest; that made of grey spheres is the second largest. The largest cluster represents a significant fraction of the system, but it is nonpercolating and the second largest cluster is also quite significant. These clusters consist of many singly connected bonds and exhibit random fractal interfaces, which prevent particles from forming a connected phase through the system. Even though Fig. 1(b) ($a=3$) shows a percolated structure, there are still several singly connected bonds and fractal substructures within the connected structure. The finite clusters are present as isolated islands. In Fig. 1(c) ($a=5$), the percolated phase is strongly connected and surrounds small isolated clusters. The strong connectivity between particles suggests that there exists a percolation transition *during* the deposition process for this value of a. Figure 1(d) shows one limit of this model, corresponding to $a=\infty$. This configuration is generated by placing initially one particle at the center of the system and then allowing only those particles that roll down over preadsorbed par-

ticles to adsorb on the surface.

Figure 2 shows that the saturation coverage increases with a from 0.547 to 0.691, which correspond to the saturation coverage of RSA (represented by the lower dashed line) and the saturation coverage at $a=\infty$ (represented by the upper dashed line), respectively. The saturated structure of RSA can be characterized as a distribution of nonconnected particles, while the structure corresponding to $a=\infty$ is a totally connected infinite Eden-like cluster. As shown in this figure, there is a one-to-one mapping between the saturation coverage and the tuning parameter a.

B. Critical properties along the saturation line

In order to obtain the percolation threshold $[a_c,\theta_c(a_c,\infty)]$ along the saturation line, and, subsequently, to determine the universality class of the percolation transition, we used direct analysis of the simulations as well as Monte Carlo renormalization group and finite-size scaling approaches. There is basically one independent variable along the saturation line: once a is chosen, the corresponding saturation coverage $\theta(a,\infty)$ is automatically fixed (on average). Initially, we monitored the order parameter P_∞, the susceptibility χ, and the mean size of

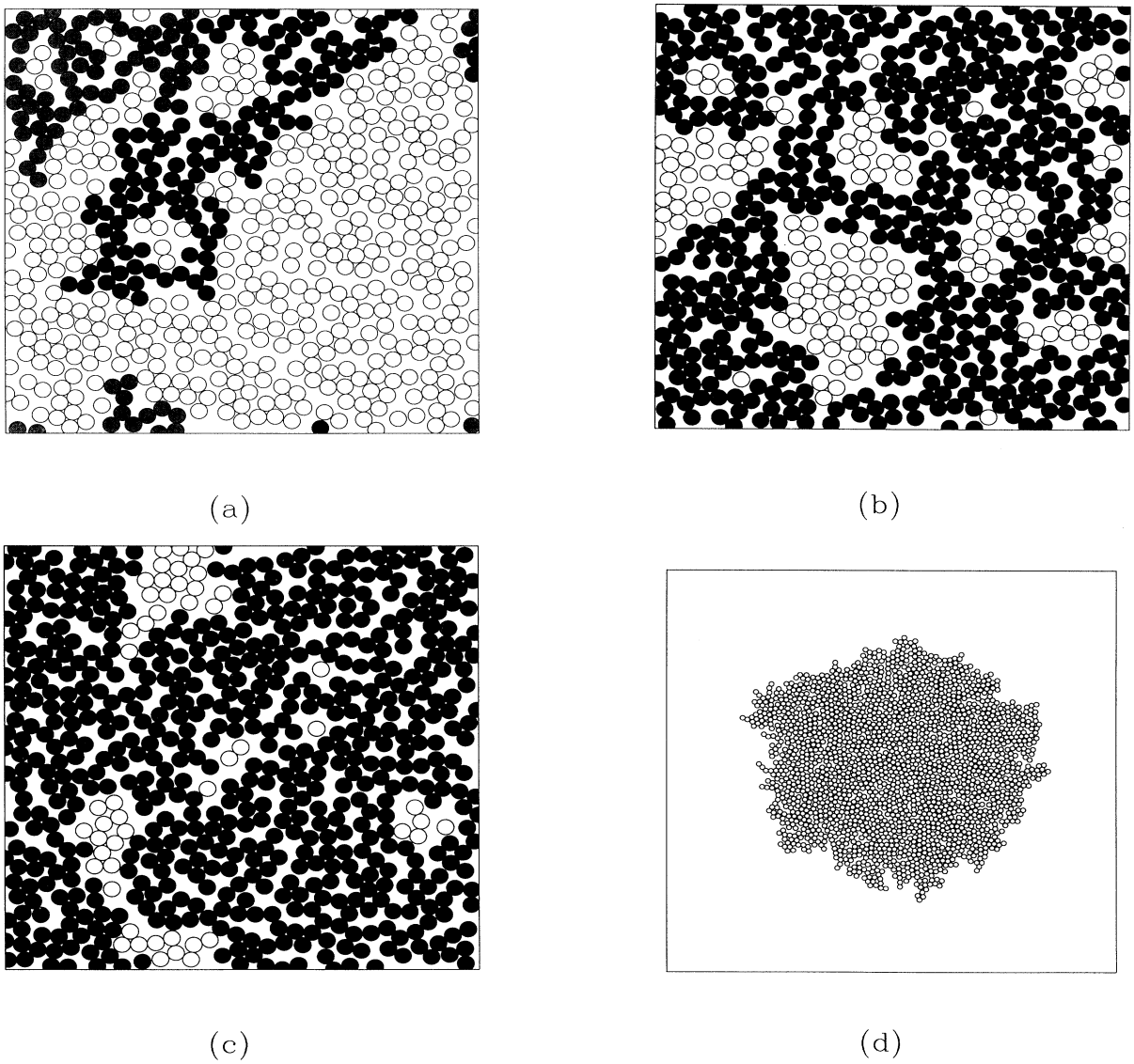

FIG. 1. Saturated configurations of spherical particles generated by the (2+1)-dimensional GBD model with different values of the tuning parameter: (a) $a=1$, (b) $a=3$, and (c) $a=5$. The black, gray, and white particles belong to the largest, the second largest, and small isolated clusters, respectively. (d) Configuration of a growing colony generated by (2+1)-dimensional GBD when $a=\infty$. The number of deposited particles is 1000.

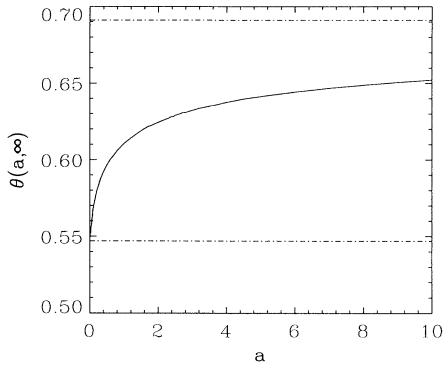

FIG. 2. Saturation coverage $\theta(a,\infty)$ (solid curve) as a function of a in the 2D GBD model. The upper and lower dashed lines represent the saturation coverages at $a=\infty$ and $a=0$, respectively.

the finite clusters S for configurations of deposited spheres at saturation as a function of a for the largest studied system size, i.e., $r_a=0.0001$. The critical behavior of these three functions in the vicinity of the percolation threshold is described by power law singularities. Following Gawlinski and Stanley [27], we treat $\theta_c(a_c,\infty)$ as an adjustable parameter and determine its value from the best correlation between the simulation data and Eqs. (5) and (6). In this way, we find the saturation coverage at the critical point $\theta_c(a_c,\infty)=0.633$, and a corresponding value of $a_c=3.128$ (or $p_c=0.758$).

From a linear fitting of the raw data on the double logarithmic plot for P_∞ and χ as functions of $[\theta(a,\infty)-\theta_c(a_c,\infty)]$ (Fig. 3), we determined the corresponding critical exponents,

$$\beta=0.14\pm0.01\ , \tag{23}$$

$$\gamma=\begin{cases}2.35\pm0.03\ , & \theta<\theta_c \\ 2.35\pm0.18\ , & \theta>\theta_c\ .\end{cases} \tag{24,25}$$

These values are in good agreement with the exact exponents of the usual two-dimensional lattice percolation: $\beta=\frac{5}{36}=0.1388\ldots$, $\gamma=\frac{43}{18}=2.388\ldots$. In accordance with the work of Lee and Torquato [32], we obtain better estimates of the exponents by considering the susceptibility χ rather than the mean cluster size S: For the latter, the estimated numerical value of $\gamma=2.21\pm0.03$.

As shown in Fig. 4, the double logarithmic plot of $|\theta_c(a_c,\infty)-\theta(a,\infty)|$ versus $|p_c-p|$ is well fitted by a straight line with slope 1,

$$|\theta_c(a_c,\infty)-\theta(a,\infty)|\sim|p_c-p|\ ,\quad \text{as } p\to p_c\ . \tag{26}$$

As discussed in Sec. III, this confirms the expected result that for any finite value of a (or $p<1$), the saturation coverage is an analytic function of a (and p). We can use then the probability p, which is a controllable parameter in the simulations, in place of the saturation coverage $\theta(p,\infty)$ in order to investigate the critical behavior.

An alternative method to estimate $\theta_c(p_c,\infty)$, p_c, and ν is obtained by combining the Monte Carlo renormalization group with finite-size scaling [25]. The central quantity in this approach is the so-called connectivity function, which describes how the occupation probability (in our case the surface coverage) is transformed under a rescaling of all lengths. In practice, the connectivity function $R(b,\theta)$ is taken as the probability that a spanning cluster is found in a $b\times b$ cell when the surface coverage is θ. Renormalization group analysis and finite-size scaling then predict that, except for special cases and connectivity rules [33], the approximate fixed point of the transformation, defined by

$$\theta^*(b)=R(b,\theta^*(b))\ , \tag{27}$$

approaches the percolation threshold as

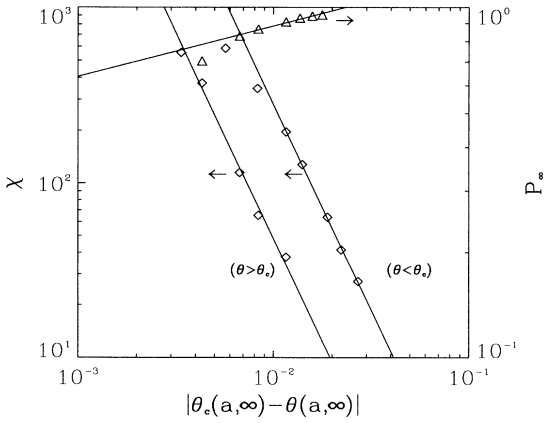

FIG. 3. Double logarithmic plot showing the dependence of $P_\infty(a,\infty)$ and $\chi(a,\infty)$ on $|\theta_c(a_c,\infty)-\theta(a,\theta)|$ along the saturation line. The relative area of a particle to the simulation cell, r_a, is 0.0001. The deviation of several points from the solid line is a finite-size effect.

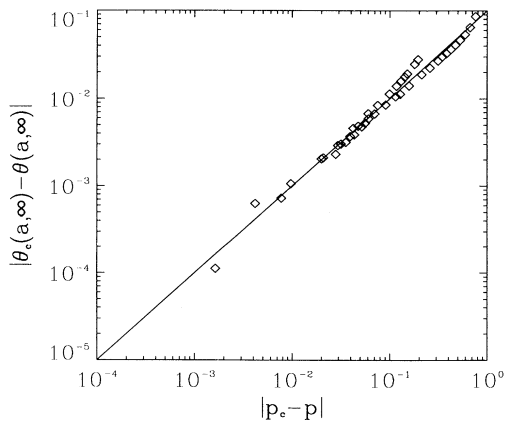

FIG. 4. Double logarithmic plot showing the relation between $|\theta_c(a_c,\infty)-\theta(a,\infty)|$ and $|p_c-p|$ along the saturation line in the $(2+1)$-dimensional GBD model. The slope of the solid line is 1.

$$\theta^*(b) \simeq \theta_c + A b^{-1/\nu} , \quad b \to +\infty , \tag{28}$$

whereas the eigenvalue of the linearized transformation,

$$\lambda_b = \left. \frac{dR(b,\theta)}{d\theta} \right|_{\theta^*(b)} , \tag{29}$$

allows a determination of the correlation length exponent ν through the relation,

$$\ln(\lambda_b) \simeq \frac{1}{\nu} \ln b + B , \quad b \to +\infty . \tag{30}$$

Since the saturation coverage θ is not a controllable simulation parameter, it is more convenient to use p. $R(b,p)$ is then the fraction of all generated GBD configurations with fixed parameter p that are at saturation in a $b \times b$ cell and possess a spanning cluster across the cell. We determined p_c and ν in two ways. The first one is to treat p as θ and use all the above equations, Eqs. (27)–(30), to obtain p_c and ν. The interpretation of the approximate fixed point $p^*(b)$ in terms of an effective real-space renormalization group approach is far from obvious, but we expect that, by virtue of the scaling laws and the fact that $R(b,p)$ tends to a Heaviside function $H(p-p_c)$ when $b \to +\infty$, Eqs. (28) and (30) still hold. A second procedure to obtain p_c and ν is to renormalize $b \times b$ cells onto a $b' \times b'$ cell and to study the approximate critical point $p^*_{b,b'}$ and the eigenvalue of the linearized transformation, $\lambda_{b,b'}$, which are defined by

$$R(b,p^*_{b,b'}) = R(b',p^*_{b,b'}) , \tag{31}$$

$$\lambda_{b,b'} = \left[\frac{dR(b,p)}{dp} \right]_{p^*_{b,b'}} \Big/ \left[\frac{dR(b',p)}{dp} \right]_{p^*_{b,b'}} . \tag{32}$$

These two quantities have an asymptotic behavior given by Eqs. (28) and (30), respectively, provided b is replaced with (b/b'). Such a method was successively applied to the continuum percolation [25].

Figure 5 shows the connectivity function $R(b,p)$ for various cell sizes. From the plot of $\ln(\lambda_b)/\ln b$ versus $1/\ln b$ [Fig. 6(a)] and that of $\ln(\lambda_{b,b'})/\ln(b/b')$ versus $1/\ln(b/b')$ for $b'=11.28$ [Fig. 6(b)], we obtain the following estimates of the correlation length exponent:

$$\nu = 1.37 \pm 0.01 \tag{33}$$

and

$$\nu = 1.35 \pm 0.01 , \tag{34}$$

respectively, which are close to the exact lattice percolation value, $\nu = \frac{4}{3} = 1.333\ldots$. From the above values of ν and Eqs. (26) and (28), we also determined the percolation threshold p_c [see, Fig. 6(c) and 6(d)]. The two different procedures give slightly different values,

$$p_c = 0.748 \pm 0.003 \tag{35}$$

and

$$p_c = 0.757 \pm 0.004 , \tag{36}$$

corresponding to $a_c = 2.975$ and $a_c = 3.122$, respectively.

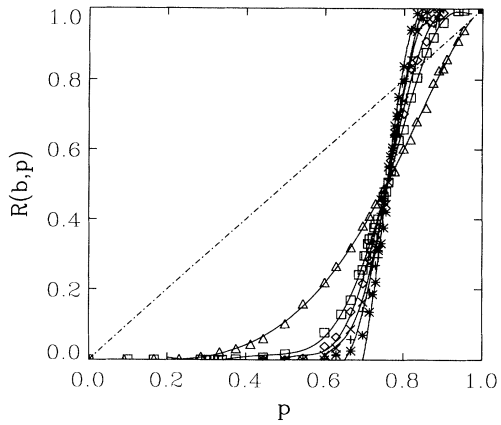

FIG. 5. Dependence of the connectivity function $R(b,p)$ on p at saturation for various cell sizes: △, $b=12.53$; □, $b=28.02$; ◇, $b=39.63$; ×, $b=51.17$; +, $b=62.67$; and ∗, $b=88.62$. The intersection of these curves with the line $p'=p$ (dashed) gives the approximate fixed point $p^*(b)$ of the transformation R. The slope of $R(b,p)$ at $p^*(b)$ is the eigenvalue λ_b from which we calculate the exponent ν.

These estimates are slightly smaller than the threshold obtained by direct analysis of the simulations ($a_c = 3.128$). Since the saturation coverage is an increasing function of a, this indicates, as expected, that analysis of a finite system overestimates the percolation threshold.

Finally, we also used finite-size-scaling relations at the percolation threshold to evaluate the critical exponents. The order parameter, which we take in a finite system as the probability for a particle to belong to the largest cluster, behaves as

$$P(p_c,L) \sim L^{-\beta/\nu} , \tag{37}$$

where L is identical to b in the preceding analysis and $p_c = 0.758$. Figure 7 shows the double logarithmic plot of the order parameter $P(p_c,L)$ (represented by triangular points) versus system size L for $p_c = 0.758$. The slope of this curve gives $\beta/\nu = 0.104 \pm 0.017$, which shows a good agreement with the lattice value, $\beta/\nu = \frac{5}{48} = 0.104\ldots$. Similarly, the mean cluster size obeys the following relation:

$$S(p_c,L) \sim L^{\gamma/\nu} , \tag{38}$$

and from the double logarithmic plot in Fig. 7, we obtain the value $\gamma/\nu = 1.799 \pm 0.046$ to be compared to the lattice value $\gamma/\nu = \frac{43}{24} = 1.791\ldots$.

From the above results, we conclude that for the $(2+1)$-dimensional GBD model along the saturation line, a percolation transition occurs at $a_c \simeq 3.05 \pm 0.07$ and belongs to the universality class of ordinary two-dimensional lattice percolation.

C. Percolation phase diagram

Having determined the critical value a_c at which percolation first occurs in the 2+1-dimensional GBD model,

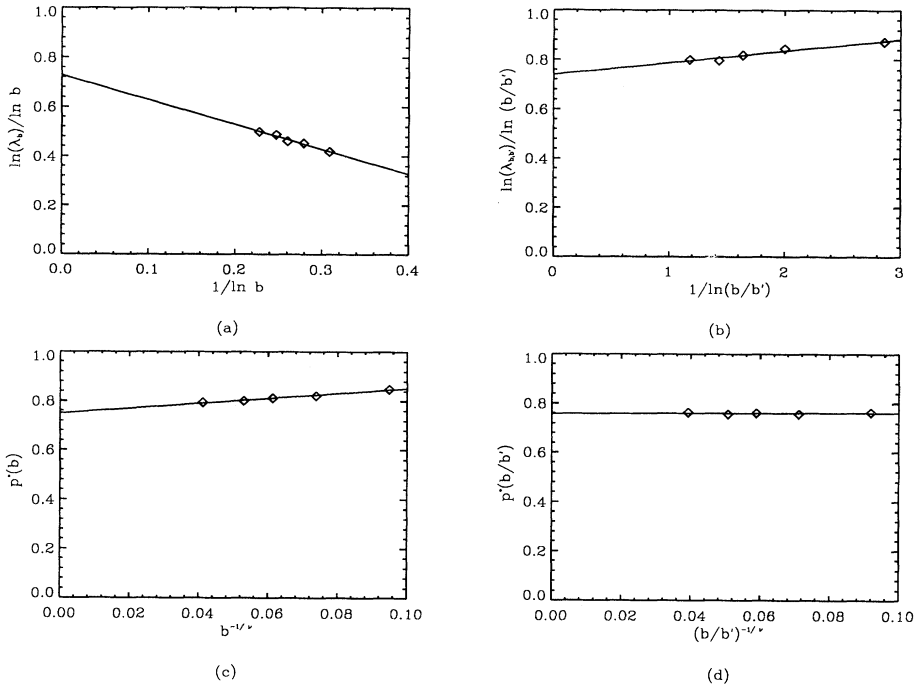

FIG. 6. (a) $\ln\lambda_b/\ln b$ versus $1/\ln(b)$; the extrapolated value for an infinite system is $1/\nu(\infty)=0.7284\pm0.0006$. (b) $\ln\lambda_{b,b'}/\ln(b/b')$ versus $1/\ln(b/b')$ for $b'=12.53$. The extrapolated value for an infinite system is $1/\nu(\infty)=0.7393\pm0.009$. (c) Finite-size scaling extrapolation of $p^*(b)$ with respect to $b^{-1/\nu}$; the critical value is $p_c=p^*(\infty)=0.748\pm0.003$. (d) Same analysis for $p^*_{b,b'}$ as a function of $(b/b')^{-1/\nu}$; $p_c=p^*(\infty)=0.757\pm0.004$.

we can study the percolation behavior for values of $a>a_c$. The system is then expected to percolate at a surface coverage $\theta_c(a)$, which is less than the saturation value $\theta(a,\infty)$ (the transition thus takes place at a finite time during the deposition process). We repeated part of the preceding analysis in order to determine the surface coverage at the percolation threshold for various values of $a>a_c$.

For every chosen value of a and for a given system size ($r_a=0.0001$), we monitored the order parameter P_∞, the susceptibility χ, and the mean mass of the finite cluster S, for configurations of spheres at different stages of the deposition process (all averages were obtained at constant surface coverage rather than at constant time). From double logarithmic plots of the data and Eqs. (5) and (6), we found the percolation threshold $\theta_c(a)$ for each chosen value of a. We also obtained the estimate of the exponent γ ($\gamma=2.295\pm0.014$ when $a=5$, $\gamma=2.367\pm0.012$ when $a=10$), which confirms that the percolation transition of the GBD model is always in the universality class of ordinary lattice percolation. We obtained rather poor estimates of the exponent β ($\beta=0.106\pm0.003$ at $a=10$), however. The percolation line $\theta_c(a)$ is shown in Fig. 8, together with the saturation line, $\theta(a,\infty)$. Both lines meet at $a=a_c\simeq3$ and $\theta_c(a)$ decreases monotonically with increasing a. A similar diagram was obtained by Evans and Sanders [34] through the study of monomer filling with nearest-neighbor exclusion on a square lattice with a biased adsorption rate, $k_\pm=(1\pm\delta)k$. For δ less than a critical value δ_c, they found a "virtual percolation threshold" corresponding to coverages higher than the saturation value of the physical adsorption model ($\delta=0$). This threshold can be obtained by extrapolating the variation of the mean cluster size S and of the correlation length ξ beyond the jamming limit. We did the same for our GBD model, i.e., we extrapolated $P_\infty(\theta)$ and $S(\theta)$ beyond the saturation coverage according to Eqs. (5) and (6) for different values of a below the critical value a_c (in practice, $a=1,2,2.5$). The resulting "virtual percolation line" is plotted in Fig. 8. Note that for small values of a (and *a fortiori* for RSA, $a=0$), the extrapolation procedure cannot provide any realistic value since the clusters are small even at saturation (or even nonexistent for RSA).

V. STRUCTURE

We have also investigated the structural characteristics of the deposited configurations by computing the radial

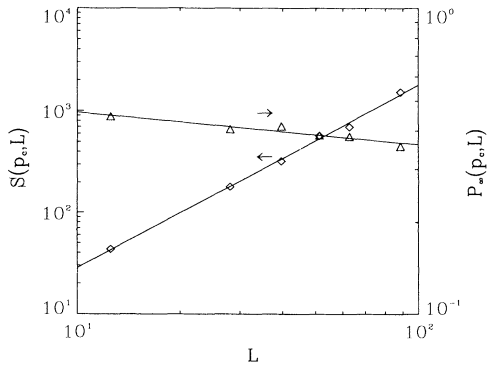

FIG. 7. Double logarithmic plot showing the dependence on L of $S(p_c,L)$ and $P_\infty(p_c,L)$. Finite-size scaling predicts that the data should be linear with slopes γ/ν and $-\beta/\nu$, respectively. $\Diamond$, $S(p_c,L)$; $\triangle$, $P_\infty(p_c,L)$.

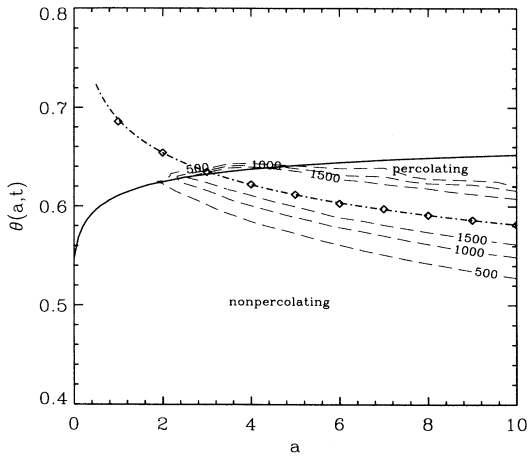

FIG. 8. Percolation phase diagram for the (2+1)-dimensional GBD model. The upper solid line represents the saturation coverage $\theta(a,\infty)$. The diamonds represent the percolation thresholds obtained from the analysis described in Sec. IV C and the dot-dashed line is a second order polynomial fit of these percolation threshold values. The multitude of dashed lines represent the contour plot of the mean cluster size S.

distribution function $g^{(2)}(r,a,\theta)$ and the pair connectedness function $P(r,a,\theta)$ above and below the percolation threshold. The latter is defined as the probability that two particles at a distance r belong to the same cluster. The mean cluster size is directly related to the pair connectedness function through

$$S(a,\theta)=1+\frac{8\theta}{\sigma^2}\int_0^\infty dr\, rP(r,a,\theta)\ . \tag{39}$$

For $a=0.5$, Fig. 9(a) shows that the pair connectedness function diminishes rapidly with r even at saturation. This reflects the short ranged connectedness between particles. Of course, the δ peak at $r=1$ is distinctive of the rolling mechanism and the peak at $r=2$ results from rolling of an incoming sphere on a dimer. There is also a small peak at $r=\sqrt{3}$, which is produced by a rolling process on a connected trimer. As a increases, the amplitude of the three peaks as well as the pair connectedness function gradually increase and show long range correlations. Around the percolation threshold [$a=3$, Fig. 9(b)], the pair connectedness function at saturation does not decrease significantly with r, which is a signature of the percolation phenomenon. On the contrary, the curves at low and intermediate coverage are gradually diminishing, thus reflecting the finiteness of the clusters. In case of $a=20$ [Fig. 9(c)], the pair connectedness function and the radial distribution function at saturation exhibit almost the same patterns and values. This means that almost all particles belong to the infinite cluster, which is similar to an Eden cluster.

We have also calculated the coordination number Z,

$$Z(a,\theta)=\frac{8\theta}{\sigma}G(a,\theta)\ , \tag{40}$$

where $G(a,\theta)$ denotes the amplitude of the singular of $g^{(2)}(r,a,\theta)$ at $r=1$. Figure 10 shows that Z gradually increases along the saturation line to approach a limiting value corresponding to that of 2D ballistic aggregation. A value of $Z>2$ is a necessary, but not sufficient, condi-

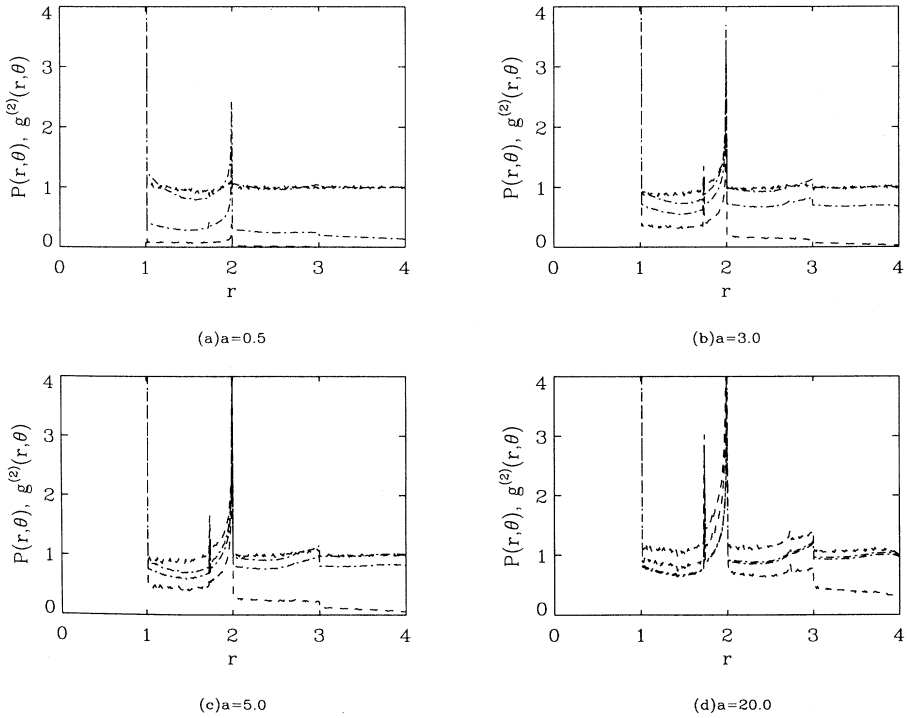

FIG. 9. Pair-correlation (upper two) and pair-connectedness (lower two) curves for (2+1)-dimensional GBD for various values of a and θ, where the distance $r=1$ means a particle diameter (σ). (a) $a=0.5$, (b) $a=3.0$, (c) $a=5.0$, and (d) $a=20.0$. — — —: $\theta=0.2$; —·—·—·: $\theta=\theta(a,\infty)$ (saturation coverage).

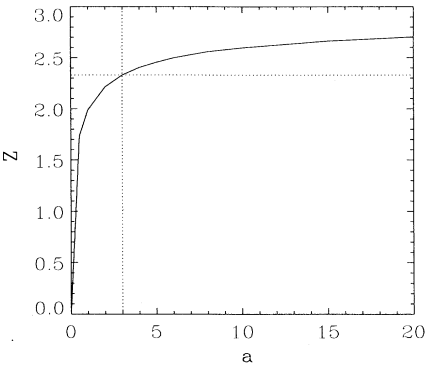

FIG. 10. Dependence of the coordination number Z at saturation on a. The intersection of the two dotted lines represents the percolation threshold, where $Z=2.33$.

tion for percolation. Table I displays the coordination numbers calculated at the percolation transition line of Fig. 8. While the coverage on the percolation transition line decreases with increasing a, the coordination number keeps increasing.

VI. CONCLUSION

We have investigated the percolation behavior of spherical particles irreversibly deposited by a generalized ballistic deposition model. The critical exponents have been obtained analytically for $(1+1)$-dimensional and numerically for $(2+1)$-dimensional by different techniques. The results show that the percolation transition of this model belongs to the universality class of ordinary lattice percolation. By investigating the system as a function of surface coverage θ and restructuring parameter a, we have constructed the full percolation diagram of the $(2+1)$-dimensional model. Percolation occurs at saturation for a critical value of a, $a_c \simeq 3.05$, and for increasing values of $a > a_c$, the transition takes place at decreasing surface coverage. We have also examined the structural properties of the layer of deposited particles for various values of a and θ by calculating both the pair correlation and pair connectedness functions.

TABLE I. Coordination number Z on the percolation transition line.

a	Z
3	2.3301
4	2.3694
5	2.4198
6	2.4393
7	2.4657
8	2.4789
9	2.4973
10	2.5059

ACKNOWLEDGMENT

We thank H. Nakanishi for very useful discussions. The Laboratoire de Physique Théorique des Liquides is Unité de Recherche Associée No. 765 au Centre National de la Recherche Scientifique.

[1] H. E. Stanley and N. Ostrowsky, in *On Growth and Form: Fractal and Non-Fractal Patterns in Physics,* edited by H. E. Stanley and N. Ostrowsky (Martinus Nijhoff, Boston, 1986), p. 79.
[2] T. Vicsek, in *Fractal Growth Phenomena,* edited by T. Vicsek (World Scientific, Singapore, 1989), p. 190.
[3] J. W. Evans, Rev. Mod. Phys. **65**, 1281 (1993).
[4] J. Feder, J. Theor. Biol. **87**, 237 (1980); J. Feder and I. Giaever, J. Colloid Interface Sci. **78**, 144 (1980).
[5] G. Y. Onoda and E. G. Liniger, Phys. Rev. A **33**, 715 (1986).
[6] Z. Adamczyk, M. Zembala, B. Siwek, and P. Warszyński, J. Colloid Interface Sci. **140**, 123 (1990); Z. Adamczyk, B. Siwek, M. Zembala, and P. Belouschek, Adv. Colloid Interface Sci. **48**, 151 (1994).
[7] J. Ramsden, Phys. Rev. Lett. **71**, 295 (1993); J. Stat. Phys. **73**, 853 (1993).
[8] P. Schaaf and J. Talbot, Phys. Rev. Lett. **62**, 175 (1989).
[9] P. Wojtaszczyk, P. Schaaf, B. Senger, M. Zembala, and J. C. Voegel, J. Chem. Phys. **99**, 7198 (1993).
[10] J. Talbot and S. Ricci, Phys. Rev. Lett. **68**, 958 (1992).
[11] R. Jullien and P. Meakin, J. Phys. A **25**, L189 (1992).
[12] A. P. Thompson and E. D. Glandt, Phys. Rev. A **46**, 4639 (1992).
[13] H. S. Choi, J. Talbot, G. Tarjus, and P. Viot, J. Chem. Phys. **99**, 9296 (1993).
[14] M. Eden, in *Proceedings of the Fourth Berkeley Symposium on Mathematical, Statistics and Probability,* edited by J. Neyman (University of California Press, Berkeley, 1961), Vol. 4, p. 223.
[15] M. J. Vold, J.Colloid Sci. **18**, 684 (1963); **14**, 168 (1959); J. Phys. Chem. **63**, 1608 (1959); **64**, 1616 (1959).
[16] P. Viot, G. Tarjus, and J. Talbot, Phys. Rev. E **48**, 480 (1993).
[17] G. Tarjus, P. Viot, H. S. Choi, and J. Talbot, Phys. Rev. E **49**, 3239 (1994).
[18] A. Bunde and S. Havlin, in *Fractals and Disordered Systems,* edited by A. Bunde and S. Havlin (Springer-Verlag, Berlin, 1991), p. 51.
[19] D. Stauffer and A. Aharony, in *Introduction to Percolation Theory,* edited by D. Stauffer and A. Aharony (Taylor & Francis, London, 1992), p. 1–114.
[20] R. Zallen, in *The Physics of Amorphous Solids,* edited by R. Zallen (Wiley, New York, 1983), p. 135.
[21] H. Gould and J. Tobochnik, *An Introduction to Computer Simulation Methods: Applications to Physical Systems Part 2* (Addison-Wesley, New York, 1988), p. 398.
[22] P. J. Reynolds, H. E. Stanley, and W. Klein, Phys. Rev. B

21, 1223 (1980).
[23] T. Vicsek and J. Kertész, J. Phys. A **14**, L31 (1981).
[24] S. Torquato, J. Chem. Phys. **81**, 5079 (1984); **84**, 6345 (1986).
[25] S. B. Lee and S. Torquato, Phys. Rev. A **41**, 5338 (1990).
[26] S. B. Lee and S. Torquato, J. Chem. Phys. **89**, 6427 (1988).
[27] E. T. Gawlinski and H. E. Stanley, J. Phys. A **14**, L291 (1981).
[28] B. I. Halperin, S. Feng, and P. N. Sen, Phys. Rev. Lett. **54**, 2391 (1985); Phys. Rev. B **35**, 197 (1987).
[29] A. Bunde, H. Harder, and S. Havlin, Phys. Rev. B **34**, 3540 (1986).
[30] Y. C. Chiew, J. Colloid Interface Sci. **143**, 397 (1991).
[31] J. W. Evans, D. R. Burgess, and D. K. Hoffman, J. Chem. Phys. **79**, 5011 (1983).
[32] S. B. Lee and S. Torquato, Phys. Rev. B **42**, 4877 (1990).
[33] R. M. Ziff, Phys. Rev. Lett. **69**, 2670 (1992); A. Aharoni and J-P. Hovi, *ibid.* **72**, 1941 (1994).
[34] J. W. Evans and D. E. Sanders, Phys. Rev. B **39**, 1587 (1989).